

RESEARCH ARTICLE

Thermal Analysis of Electromagnetic Induction Heating for Cylinder-Shaped Objects

Amir Komeili Birjandi | Prashanta Dutta

School of Mechanical and Materials Engineering, Washington State University, Pullman, Washington, USA

Correspondence: Prashanta Dutta (prashanta@wsu.edu)**Received:** 6 October 2024 | **Accepted:** 7 January 2025**Funding:** This work was funded partly by the US National Science Foundation (Grant DGE 2244082).**Keywords:** Eddy current | Green's function | induction heating | Joule heating

ABSTRACT

Induction heating is one of the cleanest and most efficient methods for heating materials, utilizing electromagnetic fields induced through AC electric current. This article reports an analytical solution for transient heat transfer in a three-dimensional (3D) cylindrical object under induction heating. A simplified form of Maxwell's equations is solved to determine the heat generation inside the cylinder by calculating the current density distribution within the body. The temperature within the solid is found from the solution of the unsteady heat equation based on Green's function. Owing to multiple spatial dimensions and time, a separation of variables technique is used to find Green's function. In addition, an innovative algorithm is proposed to take care of the variable material properties in analytical treatment. The analytical solution for temperature is verified with the data obtained from experiments for identical operating conditions. The analytical solution is used to study the impact of heat transfer coefficient and input AC current frequency and amplitude during transient heat diffusion. Our analytical solution suggests that the temperature-dependent material properties significantly affect the thermal response within the solid. Unlike many other conventional heating methods, the thermal boundary condition changes with time in induction heating, which makes our solution much more challenging.

1 | Introduction

Industrial heating is an essential aspect of manufacturing, accounting for approximately two-thirds of the energy needs in industry and close to one-fifth of worldwide energy usage. Traditionally, this heat has been generated through fossil fuel combustion, contributing substantially to industrial CO₂ emissions. As industrial heat demand rises, so does its share of CO₂ emissions, posing unique challenges for decarbonization initiatives. With the continued growth of global industrialization, there is a growing need for efficient and sustainable heating solutions. One promising approach is induction heating, which is widely recognized as one of the cleanest techniques to generate

heat in conductive materials [1]. Its adoption can significantly reduce the environmental impact of industrial processes, which aligns with global efforts to achieve climate stabilization and cleaner air [2].

The primary mechanism of induction heating is electromagnetic induction, wherein an alternating current (AC) is allowed to pass through an external coil, generating a fluctuating magnetic field within the object of interest [3, 4]. These magnetic fields induce localized electrical currents within the object [5], known as eddy currents, which generate heat through a process termed Joule heating [6, 7]. The efficiency and effectiveness of induction heating are significantly influenced by the strength

of the magnetic field and the electrical resistance of the metal, with higher resistance metals exhibiting greater ease of heating compared to their lower-resistance counterparts [8, 9]. Several elements influence the efficiency and effectiveness of induction heating, including the AC frequency, the workpiece's electrical and magnetic properties, and the induction coil design [10]. Higher frequencies often create faster heating rates and are best suited for surface heating or heating of small objects, whereas lower frequencies are employed for deeper penetration in larger workpieces [11].

Induction heating has various advantages over conventional heating technologies, including rapid heating, precise control over the heating process, energy economy [12], and the ability to heat specific portions of a workpiece without impacting the entire product [13]. These advantages make induction heating a useful technology in a variety of industrial applications, such as metal hardening [14], welding [15], brazing [16], and semiconductor device fabrication [17]. Induction heating is also beneficial due to its adaptability and efficiency. It is commonly used in industrial processes such as metal melting, heat treatment, and surface hardening, where precise temperature control and efficient heating are required to produce high-quality components [18]. Additionally, induction heating technology plays a significant role in the renewable energy sector, finding applications in the fabrication of major components for wind turbines [19], electric motors, and transformers [20].

Considering its widespread usage in industrial applications, several research groups have reported experimental studies on induction heating [21–24]. For instance, Niu et al. [25] conducted a comprehensive experimental analysis of heat transfer in two-layered packed beds of iron and graphite using a high-frequency induction furnace. Using induction heating, Aba-Perea et al. [26] compared thermoforming and forging processes for low-carbon steel double-cup parts. Tharmapalan et al. [27] presented a pancake coil design for induction heating to enhance thermal efficiency, energy performance, and uniform heat distribution. Song et al. [28] examined the induction heating process of large marine crankshaft preforms to assess temperature distribution before forging.

Experimental investigations on induction heating have various limitations and difficulties. For instance, the complexity of physical phenomena, such as interactions between electromagnetic fields and thermal processes, presents considerable obstacles to accurate measurement [29, 30]. Material properties like magnetic permeability and electrical conductivity change with temperature, confounding the problem. Precise measurement of thermal and electromagnetic parameters is difficult due to high temperatures and quick heating rates, which may result in errors. Furthermore, laboratory-scale experiments may not fully reproduce industrial-scale behaviors, and maintaining repeatability might be difficult. Environmental factors, such as ambient temperature and electromagnetic interference, also impact experimental results.

To overcome the challenges of experimental studies, a number of numerical studies have also been reported [31, 32]. For example, Hammi et al. [23] explored non-stationary induction heating through three-dimensional (3D) simulation, which is

validated against experimental observations. Using a finite element analysis, Lee et al. [33] conducted an electromagnetic and thermo-mechanical analysis of high-frequency induction heating for steel plate bending. Ostroushko et al. [34] presented a design for ablation therapy using a finite element-based numerical calculation. Utilizing ANSYS finite element software, Wu et al. [22] determined an appropriate coil structure for a shrink-fit tool holder from electromagnetic field distribution. Patidar et al. [35] used a finite element method to solve electromagnetic fields and unsteady temperature distribution to design helical coils for induction heating of hollow and solid cylindrical workpieces.

Numerical studies of induction heating also face several challenges. These methods often involve complex computations and require significant computational resources, making them time-consuming and costly. The precision of numerical simulations heavily relies on the numerical scheme. Meshing errors and convergence issues can affect the reliability of numerical solutions. *In contrast, analytical approaches offer a more straightforward and less resource-intensive alternative, providing explicit mathematical expressions that can yield quick insights into system behaviors.*

Recently, researchers have explored the possibilities of analytical solutions for induction heating. For instance, Li et al. [36, 37] presented an analytical solution for temperature distribution in a planar scanner induction heating considering line and point heat sources. They compared their results with numerical and experimental studies and presented the potential to broaden the analytical modeling methodology to a wider variety of induction heating applications. *Although a closed-form analytical expression is presented for temperature in terms of error functions in their study [36], the magnitude of the heat source term depends on the numerical solution of Maxwell's equations or experimental observations.* Using a perturbation technique, Jankowski et al. [38] proposed an approximate analytical solution for induction heating of a solid cylindrical workpiece inside a cylindrical induction coil. They presented an analytical expression for the magnetic field based on simplified Maxwell's equations and provided a framework for temperature distribution within the solid using a lumped capacitance method. Abdi et al. [39] introduced an innovative analytical coupling method between magnetic and thermal phenomena to design permanent magnet linear induction heating devices for non-magnetic parallelepiped workpieces, which could be used for fast analysis and design. Mussi et al. [40] developed an analytical solution for temperature distribution in a bimetallic plate during short-term induction heating under a non-stationary electromagnetic field. *Although analytical solutions are provided either for temperature distribution from energy equation or for electromagnetic fields to compute the Joule heating term, no studies provided closed-form analytical solutions for both electromagnetic and thermal problems occurring during induction heating.*

This study presents an analytical methodology for modeling the transient heat conduction within a 3D cylinder-shaped object undergoing induction heating. The primary aim is to obtain the temperature distribution throughout the object during the heating process, considering the electromagnetic field-induced Joule heating. Our analysis begins by solving a simplified form of Maxwell's equations to determine the heat generation inside the cylinder. Building upon this, the unsteady heat equation

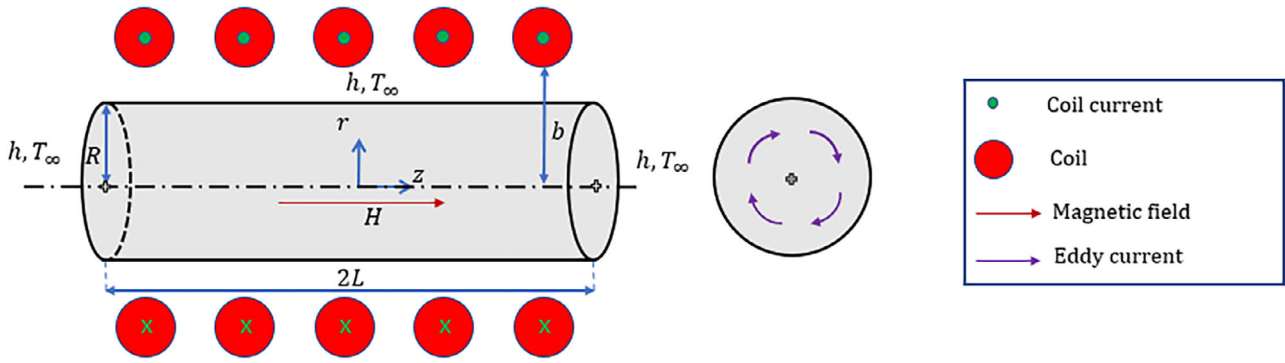


FIGURE 1 | Schematic illustration of the problem for induction heating of a solid cylindrical object of length $2L$ and radius R . An AC (alternating current) flows through the external coil with a radius of b . The total count of turns in the external coil is N . The cylindrical object is subjected to heat transfer with the surrounding air (T_∞) through convection and radiation.

was solved using Green's function. *Here, we distinguish our study from previous works by explicitly incorporating the temperature-dependent variations in the material properties and overall heat transfer coefficient. This leads to a detailed analysis of the time-dependent changes in penetration depth and the generation term, which provides a thorough understanding of the underlying heat transfer mechanisms occurring within the object. Furthermore, we have considered the spatial temperature distribution during the heating process, which is important for thick objects.* The analytical solution derived through this process is thoroughly validated by comparing it against experimental data. Finally, the verified analytical solution is used to systematically evaluate the influence of key parameters on the temperature distribution in cylindrical workpieces.

2 | Mathematical Model

In the present work, we examined the thermal response of a cylindrical object of radius R and length $2L$, which undergoes heating due to current passing through an external electric coil comprising N turns and having an internal radius b , as shown in Figure 1. The coil is energized by a sinusoidal AC current with a peak amplitude of I_p and a frequency of f (angular frequency ω). The cylinder rejects heat to the surrounding fluid of temperature T_∞ with a convection coefficient of h_c . Additionally, radiation heat transfer, which varies with temperature, is considered in this study. The surface emissivity (ϵ_R) of the cylinder is assumed as a constant. The cylinder material is considered non-magnetic, characterized by a permeability of μ .

2.1 | Governing Equations

In induction heating, the generation of eddy currents occurs when a workpiece is subjected to alternating magnetic fields induced by the flow of an AC current through the external coil, as shown in Figure 1. The electric field and current density considered for the induction heating system presented in this study are exclusively circumferential, that is, $\vec{E} = E\mathbf{e}_\theta$ and $\vec{J} = J\mathbf{e}_\theta$, whereas the magnetic field is entirely axial, which is expressed as $\vec{H} = H\mathbf{e}_z$. Hence, the scalar quantities H , E , and J (respectively) define the magnetic field, electric field, and current density. For the aforementioned electromagnetic problem, the

governing equation for the magnetic field can be derived from Ampere and Faraday laws as [41]

$$\frac{d^2H}{dr^2} + \frac{1}{r} \frac{dH}{dr} - (m^2)H = 0 \quad (1)$$

where $m^2 = j\omega\mu\sigma$ and σ represents electrical conductivity. Because the induced magnetic field generates heat in the cylinder, the temperature distribution (T) within the workpiece can be described by the unsteady heat diffusion equation with volumetric heat generation:

$$\rho c \frac{\partial T}{\partial t} = \vec{\nabla} \cdot (k \vec{\nabla} T) + \dot{q}_{\text{gen}} \quad (2)$$

where k , ρ , and c represent the thermal conductivity, density, and specific heat of the material, respectively, and \dot{q}_{gen} is the Joule heat generated per unit volume due to the movement of eddy currents within the workpiece. The Joule heat term can be given as

$$\dot{q}_{\text{gen}} = \vec{J} \cdot \vec{E}^* \quad (3)$$

where \vec{E}^* is the complex conjugate of the electric field. To acquire the temperature distribution inside the object of interest, it is essential to find the electric and magnetic fields. Next, we delve into how to calculate electric and magnetic fields from simplified Maxwell's equations.

2.2 | Analysis of Electromagnetic Field

The volumetric heat generation depends on the current density (J) in the cylindrical object, which is directly related to the induced magnetic field (H) within the object. The general solution for the magnetic field distribution inside the cylindrical object can be obtained from Equation (1) as

$$H(r) = c_1 I_0(mr) + c_2 K_0(mr) \quad (4)$$

The coefficient c_1 and c_2 can be determined by applying the appropriate boundary conditions at the centerline and outer surface of the cylinder.

For instance, the symmetry requires that the magnetic field be finite at the centerline of the cylindrical object; therefore, c_2 must

be zero. Thus,

$$H(r) = c_1 I_0(mr) \quad (5)$$

Letting $H = H_s$ at the outer surface ($r = R$), the ratio of the magnetic field at a given radius to that of the cylinder's outer surface can be obtained as

$$\frac{H(r)}{H_s} = \frac{I_0(mr)}{I_0(mR)} \quad (6)$$

The I_0 can be separated into an imaginary and a real component as

$$\frac{H(r)}{H_s} = \frac{ber(mr) + j bei(mr)}{ber(mR) + j bei(mR)} \quad (7)$$

where ber and bei are the Kelvin functions [41]. For a short coil, the magnetic field at the exterior surface of the cylinder can be estimated as

$$H_s = nIK_n \quad (8)$$

where I is the RMS (root mean square) amplitude of the current and n is the number of coil turns per unit length. The modified Nagaoka coefficient K_n can be given as [42]

$$K_n = \bar{K}_n \left(1 - \frac{R^2}{b^2}\right) + \frac{R^2}{b^2} \quad (9)$$

For a finite-length coil, the Nagaoka coefficient \bar{K}_n can be estimated as

$$\bar{K}_n = \frac{1 + 1.535604\beta^2 + 0.273728\beta^4}{1 + 1.035808\beta^2} - \frac{8\beta}{3\pi} \quad (10)$$

where $\beta = b/2L$. Thus, one can find the magnetic field at any radial location in terms of penetration depth (δ) as

$$H(r) = H_s \frac{ber\left(\sqrt{2}\frac{r}{\delta}\right) + j bei\left(\sqrt{2}\frac{r}{\delta}\right)}{ber\left(\sqrt{2}\frac{R}{\delta}\right) + j bei\left(\sqrt{2}\frac{R}{\delta}\right)} \quad (11)$$

where $\delta = \sqrt{\frac{2}{\omega\mu\sigma}}$, which estimates how deep an electromagnetic wave can penetrate into a conductor before it is significantly attenuated. Once the surface magnetic field (H_s) is known, the current density in the cylinder can be calculated from

$$J = \nabla \times H = -\left(\frac{\partial H}{\partial r}\right) \hat{e}_\theta \quad (12)$$

Substituting Equation (11) into Equation (12), we have

$$J = -\left(\frac{\sqrt{2}H_s}{\delta}\right) \left(\frac{ber'\left(\sqrt{2}\frac{r}{\delta}\right) + j bei'\left(\sqrt{2}\frac{r}{\delta}\right)}{ber\left(\sqrt{2}\frac{R}{\delta}\right) + j bei\left(\sqrt{2}\frac{R}{\delta}\right)}\right) \hat{e}_\theta \quad (13)$$

Utilizing Equation (3) in conjunction with the relationship $E^* = \rho_e J^*$, the heat produced by the electromagnetic field induced

eddy currents in the cylindrical object can be presented as

$$\dot{q}_{\text{gen}} = \left(\frac{2\rho_e H_s^2}{\delta^2}\right) \left(\frac{ber'^2\left(\sqrt{2}\frac{r}{\delta}\right) + bei'^2\left(\sqrt{2}\frac{r}{\delta}\right)}{ber^2\left(\sqrt{2}\frac{R}{\delta}\right) + bei^2\left(\sqrt{2}\frac{R}{\delta}\right)}\right) \quad (14)$$

2.3 | Analysis of Temperature Distribution

Unlike the lumped capacitance method, which assumes a uniform temperature throughout the body and oversimplifies the transient heat conduction problem, our method overcomes these limitations. In our approach, we employ the Green's function method to solve the unsteady, 3D energy equation with non-uniform generation terms throughout the object. This method provides a powerful tool for solving unsteady problems with more intricate boundary conditions. Using Green's function, one can account for various initial and nonhomogeneous boundary conditions more effectively, including scenarios with variable generation terms, and obtain a more accurate representation of the temperature distribution within the cylindrical object.

For an axisymmetric cylindrical object subjected to induction heating, the energy equation simplifies into

$$\begin{aligned} \frac{1}{r} \frac{\partial}{\partial r} \left(kr \frac{\partial T}{\partial r}\right) + \frac{\partial}{\partial z} \left(k \frac{\partial T}{\partial z}\right) + \dot{q}_{\text{gen}} \\ = \rho c \frac{\partial T}{\partial t} \text{ in } 0 \leq r < R; 0 < z < L \end{aligned} \quad (15)$$

The expression of heat generation \dot{q}_{gen} is presented in Equation (14), which depends on the permeability and conductivity of the object as well as the amplitude of the electric current flowing through the external coil and the number of coils per unit length. The initial and boundary conditions for this thermal problem are

$$T = T_0 \text{ at } t = 0 \quad (15a)$$

$$T = \text{finite at } r = 0; t > 0 \quad (15b)$$

$$-k \frac{\partial T}{\partial r} = h(T - T_\infty) \text{ at } r = R; t > 0 \quad (15c)$$

$$\frac{\partial T}{\partial z} = 0 \text{ at } z = 0; t > 0 \quad (15d)$$

$$-k \frac{\partial T}{\partial z} = h(T - T_\infty) \text{ at } z = L; t > 0 \quad (15e)$$

Here, h indicates the overall heat transfer coefficient and is defined as

$$h = h_c + h_r \quad (16)$$

In this study, the convective heat transfer coefficient h_c is considered constant; however, the radiative heat transfer coefficient h_r varies with temperature on the surface as

$$h_r = \sigma_B \epsilon_R (T_s^2 + T_\infty^2) (T_s + T_\infty) \quad (17)$$

where σ_B is the Stefan–Boltzmann constant. Because the generation term is affected by temperature-dependent material properties, the governing equation given in Equation (15) is nonlinear. Therefore, obtaining a closed-form analytical solution for this system is challenging due to its nonlinearity. However, the problem can be considered linear if we examine the temperature evolution over a very short processing time. In this short duration, the changes in material properties and penetration depth can be considered negligible due to the limited temperature variation inside the body.

Thus, over a short but finite period of time, the temperature distribution can be analytically determined using Green's function technique applied to the aforementioned second-order, nonhomogeneous partial differential equation assuming temperature-independent material properties. Subsequently, we utilize the obtained solution as the initial condition for the next time step.

The governing equation for a short induction heating period can be expressed as

$$\frac{\partial^2 \theta}{\partial r^2} + \frac{1}{r} \frac{\partial \theta}{\partial r} + \frac{\partial^2 \theta}{\partial z^2} + \frac{\dot{q}_{\text{gen}}}{k} = \frac{1}{\alpha} \frac{\partial \theta}{\partial t} \quad \text{in } 0 \leq r < R; 0 < z < L \quad (18)$$

where α is the thermal diffusivity of the object and $\theta(r, z, t) = T(r, z, t) - T_\infty$. Consequently, the boundary and initial conditions are reformulated as follows:

$$\theta = \theta_0 \text{ at } t = 0 \quad (18a)$$

$$\theta = \text{finite at } r = 0; t > 0 \quad (18b)$$

$$\frac{\partial \theta}{\partial r} + H_c \theta = 0 \text{ at } r = R; t > 0 \quad (18c)$$

$$\frac{\partial \theta}{\partial z} = 0 \text{ at } z = 0; t > 0 \quad (18d)$$

$$\frac{\partial \theta}{\partial z} + H_c \theta = 0 \text{ at } z = L; t > 0 \quad (18e)$$

where $\theta_0 = T_0 - T_\infty$ and $H_c = \frac{h}{k}$. We consider the homogeneous version of the governing equation within the same region to obtain the desired Green's function:

$$\frac{\partial^2 \psi}{\partial r^2} + \frac{1}{r} \frac{\partial \psi}{\partial r} + \frac{\partial^2 \psi}{\partial z^2} = \frac{1}{\alpha} \frac{\partial \psi}{\partial t} \quad \text{in } 0 \leq r < R; 0 < z < L \quad (19)$$

The following are the corresponding initial and boundary conditions:

$$\psi = \theta_0 \text{ at } t = 0 \quad (19a)$$

$$\psi = \text{finite at } r = 0; t > 0 \quad (19b)$$

$$\frac{\partial \psi}{\partial r} + H_c \psi = 0 \text{ at } r = R; t > 0 \quad (19c)$$

$$\frac{\partial \psi}{\partial z} = 0 \text{ at } z = 0; t > 0 \quad (19d)$$

$$\frac{\partial \psi}{\partial z} + H_c \psi = 0 \text{ at } z = L; t > 0 \quad (19e)$$

Equation (19) can be solved using the separation of variables method as

$$\psi(r, z, t) = R(r)Z(z)\Gamma(t) \quad (20)$$

where R , Z , and Γ are the function of r , z , and t , respectively. Substituting Equation (20) into Equation (19) leads to

$$\frac{1}{R} \left(\frac{d^2 R}{dr^2} + \frac{1}{r} \frac{dR}{dr} \right) + \frac{1}{Z} \frac{d^2 Z}{dz^2} = \frac{1}{\alpha \Gamma} \frac{d\Gamma}{dt} = -\lambda_{nm}^2 \quad (21)$$

where λ_{nm} are the eigenvalues. Equation (21) can be split to the following equations:

$$\frac{d\Gamma}{dt} + \lambda_{nm}^2 \alpha \Gamma = 0 \quad (22a)$$

$$\frac{d^2 Z}{dz^2} + \beta_n^2 Z = 0 \quad (22b)$$

$$\frac{d^2 R}{dr^2} + \frac{1}{r} \frac{dR}{dr} + (\eta_m^2) R = 0 \quad (22c)$$

where β_n and η_m are eigenvalues and $\eta_m^2 = \lambda_{nm}^2 - \beta_n^2$. The general solution of Equation (19) is obtained through the summation of the product solutions across all eigenvalues (β_n, η_m) as

$$\psi(r, z, t) = \sum_{n=0}^{\infty} \sum_{m=0}^{\infty} C_{nm} e^{-\alpha \lambda_{nm}^2 t} J_0(\eta_m r) \cos(\beta_n z) \quad (23)$$

where C_{nm} are the coefficients and can be found as

$$C_{nm} = \frac{\int_{z=0}^L \int_{r=0}^R r \theta_0 J_0(\eta_m r) \cos(\beta_n z) dr dz}{\left(\int_{r=0}^R r J_0^2(\eta_m r) dr \right) \left(\int_{z=0}^L \cos^2(\beta_n z) dz \right)} \quad (24)$$

Thus, using Green's function, the solution of the homogenous problem, Equation (19), becomes

$$\psi(r, z, t) = \int_{z'=0}^L \int_{r'=0}^R G(r, z, t | r', z', \tau) \Big|_{\tau=0} r' \theta_0 dr' dz' \quad (25)$$

By comparing Equations (23) and (25), the Green's function for $\tau = 0$ is as

$$G(r, z, t | r', z', \tau) \Big|_{\tau=0} = \sum_{n=0}^{\infty} \sum_{m=1}^{\infty} J_0(\eta_m r) e^{-\alpha \lambda_{nm}^2 t} \left[\frac{J_0(\eta_m r') \cos(\beta_n z') \cos(\beta_n z)}{\int_{r'=0}^R r' J_0^2(\eta_m r') dr' \int_{z'=0}^L \cos^2(\beta_n z') dz'} \right] \quad (26)$$

Replacing t in Equation (26) with $(t - \tau)$ the desired Green's function is obtained as

$$G(r, z, t | r', z', \tau) = \sum_{n=0}^{\infty} \sum_{m=0}^{\infty} J_0(\eta_m r) e^{-\alpha \lambda_{nm}^2 (t-\tau)} \left[\frac{J_0(\eta_m r') \cos(\beta_n z') \cos(\beta_n z)}{\int_{r'=0}^R r' J_0^2(\eta_m r') dr' \int_{z'=0}^L \cos^2(\beta_n z') dz'} \right] \quad (27)$$

The final solution of the nonhomogeneous problem (Equation 15) in terms of the above Green's function is obtained as

$$T(r, z, t) = T_{\infty} + \int_{z'=0}^L \int_{r'=0}^R G(r, z, t | r', z', \tau) |_{\tau=0} \theta_0 r' dr' dz' + \frac{\alpha}{k} \int_{\tau=0}^t \int_{z'=0}^L \int_{r'=0}^R G(r, z, t | r', z', \tau) \dot{q}_{gen} r' dr' dz' d\tau \quad (28)$$

The second last term in the above equation accounts for the initial condition, and the last term takes care of the internal heat generation. By substituting Equations (26), (27), and (14) into Equation (28), the distribution of temperature within the cylinder can be determined.

3 | Results and Discussion

The primary aim of this article is to provide a closed-form analytical solution for temperature during the induction heating of 3D cylindrical objects. Because induction heating is widely used across various industries, this study can improve manufacturing processes and increase efficiency. Induction heating originates from the interaction of electromagnetic fields in an object through a complex volumetric heat generation process. The generated heat during the induction heating is a function of location and time, as presented in Equation (14). Thus, the governing equation for temperature, derived from energy conservation, is nonlinear. Furthermore, temperature-dependent thermophysical properties, such as specific heat, thermal conductivity, and density, make this problem more challenging for analytical treatment. Additionally, the heat transfer from the surface, due to both convection and radiation heat transfer, is a function of surface temperature. To overcome these challenges, we developed a new technique for the unsteady solution of temperature by marching in time, similar to a numerical scheme for unsteady problems [43]. Like an unsteady numerical study, a small time step (Δt) is considered for time marching, during which all parameters (h , k , ρ , c) are assumed to be constant. Figure 2 shows the workflow to determine the temperature distribution from the applied current in the external coil. The temperature result obtained from a time step is considered the initial condition for the calculation in subsequent time steps.

Although the analytical results presented here (Equation 28) can be applicable to any conductive materials used in induction heating, in this study, temperature results are presented for POCO AXM-5Q ultrafine grain graphite [44] because of the availability of temperature-dependent material properties. Furthermore, all results are presented for a solid cylindrical object with a constant radius of 4.51 cm and a total length of 19.8 cm, though the length and radius of the object can be modified as needed. For induction heating of the cylinder, we have considered a current-carrying coil with an inner radius (b) of 6.65 cm and a total of 11 turns around the object. These geometric values are selected on the basis of the experimental setup presented by Jankowski et al. [38], although our analytical model is valid for any size cylindrical object. Table 1 presents thermophysical properties of the materials, including density, temperature-dependent specific heat, electrical

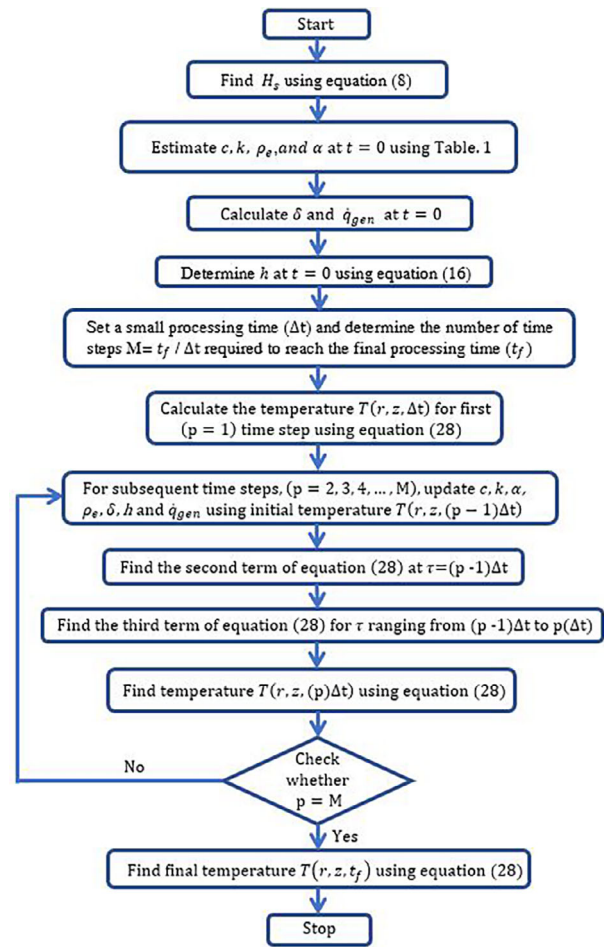


FIGURE 2 | The algorithm employed for finding temperature distribution inside a cylindrical object considering temperature-dependent properties.

TABLE 1 | Properties of POCO graphite at different temperatures [44].

T (K)	σ ($\frac{1}{\Omega m}$)	c (J/kgK)	k (W/mK)	ρ (kg/m ³)
293.15	75 250	721	120	1720
393.15	86 417	1026	108	1720
493.15	96 585	1269	95	1720
593.15	105 001	1424	88	1720
693.15	111 244	1549	80	1720
793.15	115 292	1645	75	1720
893.15	117 437	1712	70	1720
993.15	118 124	1763	66	1720
1093.15	117 807	1809	62	1720
1193.15	116 860	1855	60	1720
1293.15	115 549	1892	57	1720
1393.15	114 035	1926	56	1720
1493.15	112 396	1959	55	1720

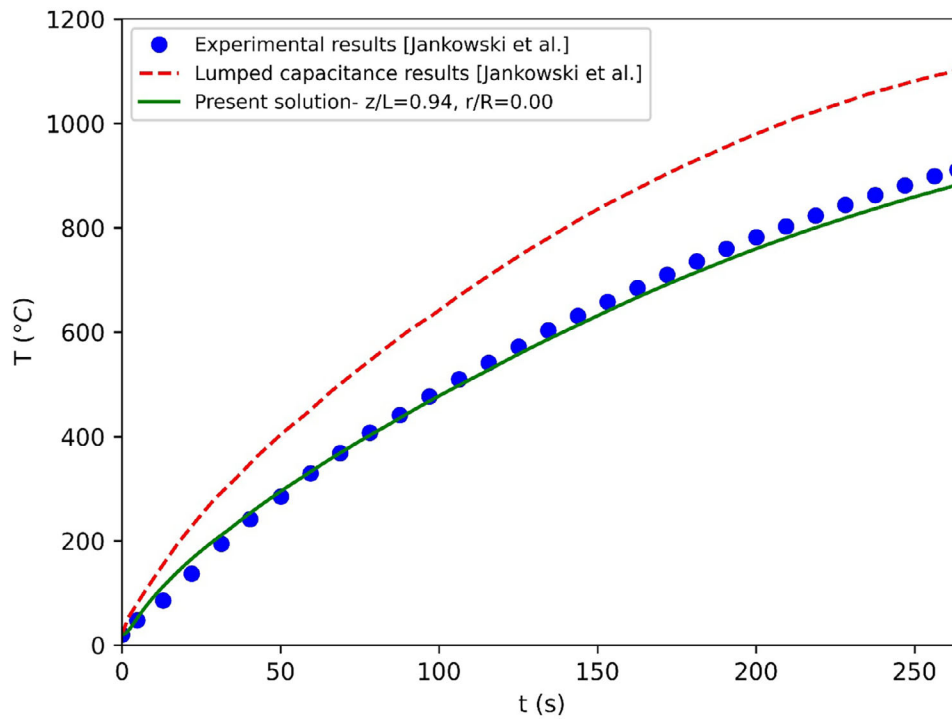


FIGURE 3 | Validation of the present analytical results with experimental data reported by Jankowski et al. [38]. Here, h_r varies with surface temperature and h_c is considered to be negligible.

TABLE 2 | Input parameters and other heat transfer properties [44].

Parameters	Values
Stefan–Boltzmann constant, σ_B (W/m ² K ⁴)	5.67×10^{-8}
Permeability, μ (H/m)	$4\pi \times 10^{-7}$
Emissivity of the surface, ε_R	0.9
Convective heat transfer coefficient, h_c (W/m ² K)	10
Frequency, f (Hz)	10 000
Ambient temperature, T_∞ (K)	298.15
Initial temperature, T_0 (K)	293.15
Current (RMS), I (A)	467.72

conductivity, and thermal conductivity. Additionally, Table 2 contains all other properties and input parameters associated with induction heating. Unless stated explicitly, the aforementioned physical dimensions and parameters are maintained throughout the article.

3.1 | Comparison With Experiments

We compared our results with previous experimental studies to effectively validate the current analytical model. Figure 3 shows the temperature comparison between our work and the experimentally reported results by Jankowski et al. [38]. We particularly selected this work for validation because it presents both experimental and numerical results with great clarity. In

their experimental work, a K type thermocouple was used to measure temperature, and the thermocouple was installed in a hole that was drilled at the center of the cylinder at $z/L = 0.94$. Thus, our analytical results are also presented at the same axial location. As depicted in Figure 3, our analytical solution matches well with the experimental observations. For comparison, we also presented their lumped capacitance-based analytical results [38]. *This direct comparison shows that a 3D model can capture the experimentally obtained temperature distribution with much better accuracy than a lumped capacitance-based method.*

The temperature increase in the object is due to the volumetric heat generation resulting from the flow of AC current through the external coil. The volumetric heat generation's magnitude is directly related to the current density and frequency of the applied electric current. Volumetric heat generation is also affected by the penetration depth, which is influenced by the material's properties. Thus, understanding the temporal evolution of penetration depth and variation of the heat generation with space and time is critical for optimizing industrial processes during induction heating. Figure 4A provides the distribution of volumetric heat generation along the radial direction during the induction heating process. As expected, the effect of heat generation is the highest at the surface, and it exponentially decays to zero at the centerline of the object. In this study, it is assumed that heat generation is uniform in the axial direction due to closely spaced coils.

The temporal dependence on the volumetric heat generation term is caused by the penetration depth variation, as shown in Figure 4B. The penetration depth depends on the frequency, the permeability, and the material's electrical conductivity. Higher conductivity materials tend to have shorter penetration depths because they absorb and dissipate electromagnetic energy more

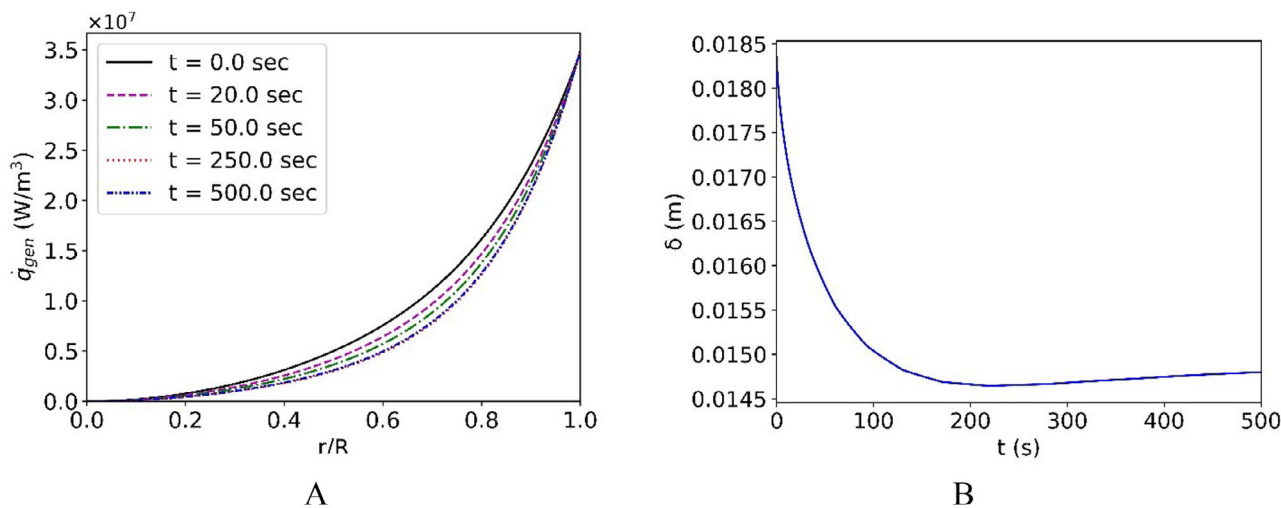


FIGURE 4 | The variations of (A) the heat generated per unit volume due to eddy current and (B) penetration depth over time. The depth of the penetration does not vary significantly after the first 200 s.

effectively. Because electrical conductivity increases with temperature in the POCO graphite, the penetration depth decreases accordingly. The penetration depth starts at a high value of approximately 18.4 mm and decreases to 14.5 mm within the first 200 s, with slight changes thereafter. This type of heating can be advantageous for applications needing high surface temperatures but requires careful control to avoid potential surface overheating. Additionally, although the changes in penetration depth become negligible after 200 s, the spatial distribution of the volumetric heat generation term does not change appreciably afterward, as shown in Figure 4A.

3.2 | Transient Evolution of Overall Heat Transfer Coefficient

As mentioned earlier, the volumetric heat generation term is the primary driving mechanism for heat in the object of interest during induction heating. The continuous increase in temperature over time, as demonstrated in Figure 3, indicates that there is a net gain of heat in the system. In other words, the heat rejection from the system is either non-existent or very minor. For the system described in the problem definition, the only mechanism for heat rejection is through the interaction between the solid object and the neighboring fluid (air). This interaction can serve a vital purpose in guiding the temperature distribution within the object. In many low surface temperature heat transfer scenarios [45–47], this interaction is primarily due to convection. However, in induction heating, the surface temperature generally reaches very high as the heating continues. Thus, the radiative heat transfer from the object to its surroundings will be another major player. Because the surface temperature increases (see Figure 3) with time, the radiation heat transfer will also change, albeit nonlinearly. To address the heat transfer between the surface and its surroundings, we have considered an overall heat transfer coefficient, incorporating radiation and convection effects. This enables us to better understand the competition between energy generation within the cylinder due to induction heating and the opposing mechanisms of radiative and convective heat transfer at the surface.

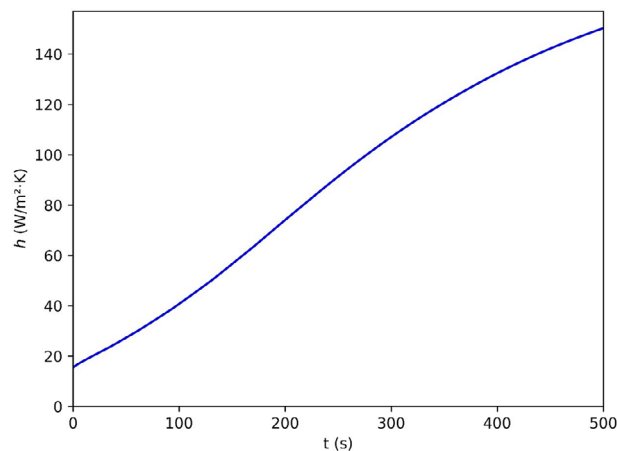


FIGURE 5 | Temporal changes in the overall heat transfer coefficient, which comprises convective and effective radiative components.

For radiation heat transfer, we have assumed a specified surface emissivity (ϵ_R) of 0.9, whereas the convective heat transfer is maintained constant ($h_c = 10$ W/m² K) based on other related work [48]. Figure 5 illustrates the transient change in the overall heat transfer coefficient, h . This nonlinear trend arises because the radiation coefficient varies with temperature during induction heating, although the convection coefficient remains constant. By controlling these heat transfer coefficients, engineers can design better cooling or heating strategies to enhance performance, reduce energy consumption, and improve the reliability of industrial processes.

3.3 | Spatial Variation in Temperature During Induction Heating

The electromagnetic field–induced heat generation is highly non-uniform (Figure 4A) in the spatial (radial) direction. This spatially varied heat generation will cause a non-uniform temperature distribution inside the object. In some industrial processes, it is essential to have uniform (or nearly uniform) temperature

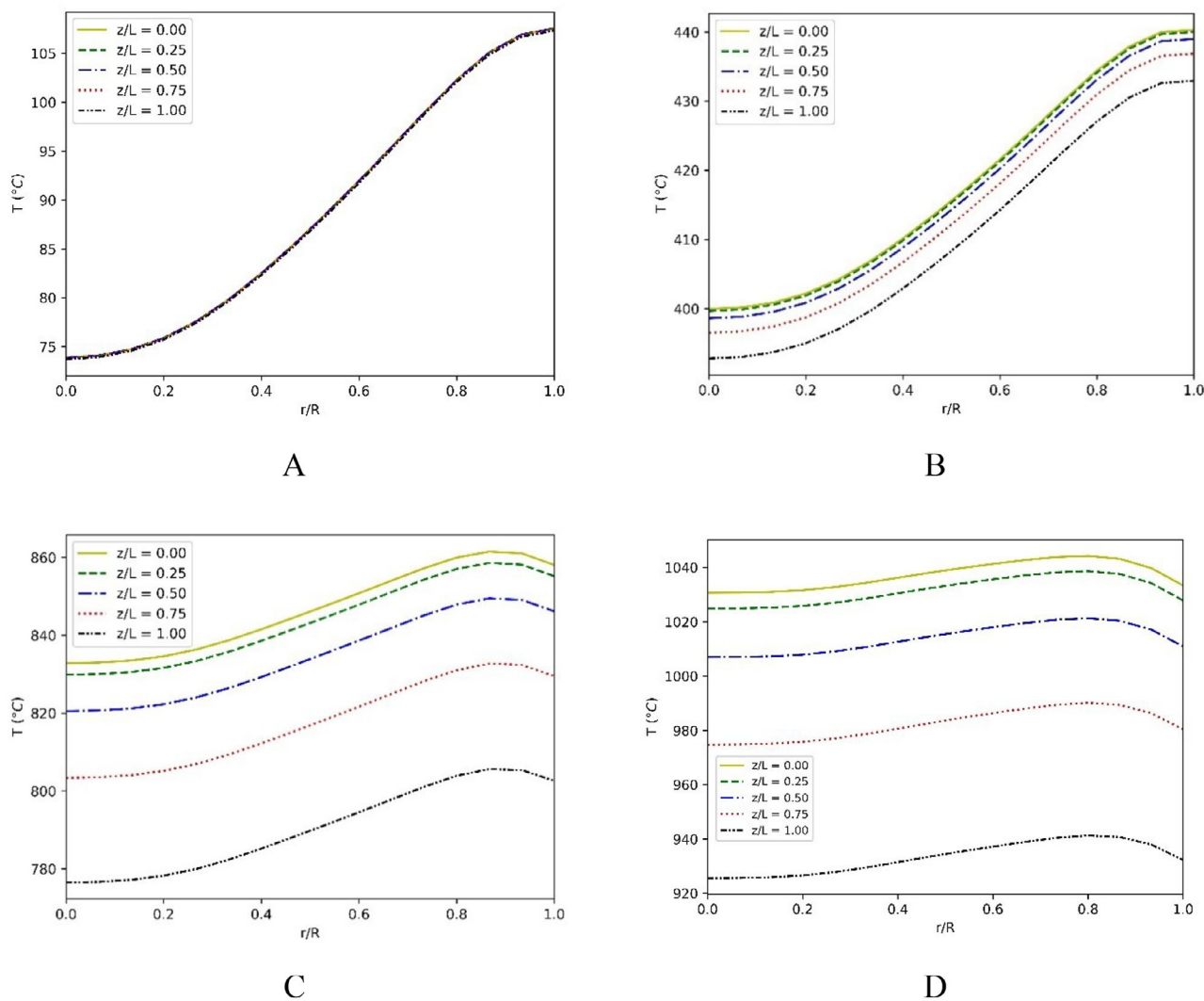


FIGURE 6 | The temperature distribution along the cylinder's radial direction for different axial positions at (A) $t = 10$ s, (B) $t = 100$ s, (C) $t = 300$ s, and (D) $t = 500$ s. Here, $f = 10$ kHz.

distribution throughout the object. For such scenarios, other competing mechanisms of heat transfer must be explored through boundaries. In the case of a solid cylinder, the only accessible boundaries for energy transfer are the outer surface (at $r = R$) and two edges (at $z = \pm L$), where heat transfer can occur through convection and radiation. To understand the effect of radiation and convection in induction heating, we have presented the distribution of temperature in the radial direction at various times for different axial locations in Figure 6.

As expected, the temperature increases with time during induction heating due to heat generation within the body. As induction heating commences, the temperature profile exhibits a disparity, with the lowest temperature observed at the core of the cylinder and the highest at its edge. This discrepancy can be explained using the volumetric heat generation during induction heating. As shown in Figure 4A, the generated heat (due to the eddy current) is much higher on the outer surface of the cylinder than at its center, resulting in higher temperatures at the outer surface. Over time, the heat diffusion from surfaces diminishes the temperature gradient, resulting in a more even temperature

distribution along the r -direction. Furthermore, a slight reduction in temperature at the outer edge region of the cylinder is observed for $t = 300$ s and beyond, as illustrated in Figures 6C,D. This phenomenon is attributed to the much higher radiation heat transfer to the surroundings as the surface temperature increases with time.

Another notable observation from this figure is that initially, there is no substantial difference in the temperature profiles along the axial direction, though temperature varies in the radial direction. However, as time progresses, there is a large temperature gradient along the axial direction due to strong radiative heat transfer from two ends (at $z = \pm L$). Thus, our analytical results, as presented in Figure 6, reveal that the temperature distribution is a strong function of location in addition to time. Hence, a lumped capacitance-based heat transfer analysis will provide an over-simplistic view of the problem. Considering significant non-uniformity in temperature both in the axial and radial direction, one should consider the spatial heat diffusion aspects in addition to non-uniform generation to accurately predict the distribution of temperature in the object during induction heating.

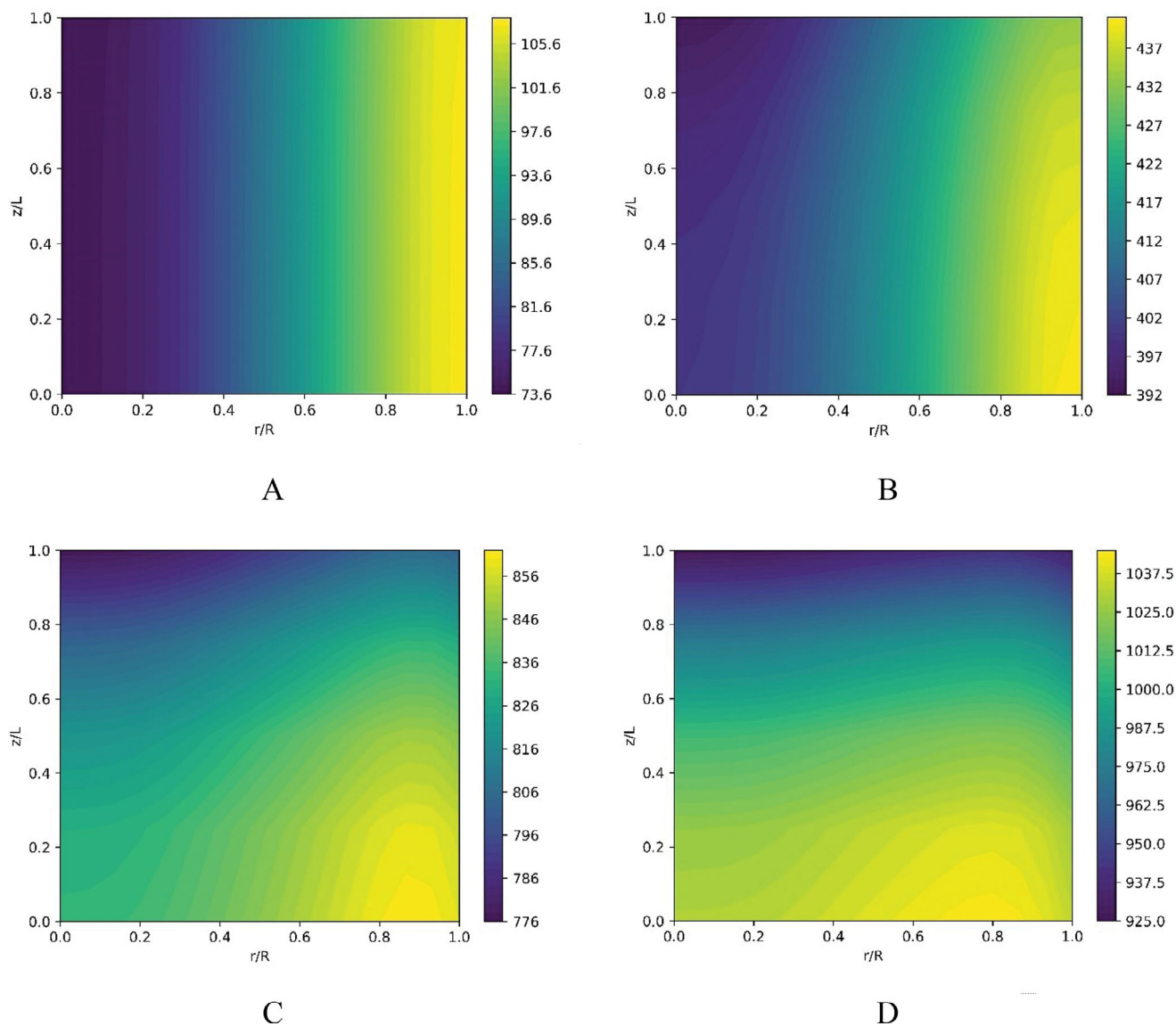


FIGURE 7 | Two-dimensional temperature contours during induction heating with an AC current (root mean square (RMS) amplitude, $I = 467.72$ A, and frequency, $f = 10$ kHz): (A) $t = 10$ s, (B) $t = 100$ s, (C) $t = 300$ s, and (D) $t = 500$ s.

To better comprehend the spatial variations, the temperature contours are presented in Figure 7 for different times (10, 100, 300, and 500 s) during the induction heating. Initially, as eddy currents generate more heat at the cylinder's edges, the higher temperature tends to concentrate toward the surface due to the skin effect. However, over time, heat penetrates deeper into the material due to higher thermal conductivity. Additionally, the impact of convective and radiative heat transfer from the edges and lateral surfaces becomes more pronounced, influencing the overall temperature distribution. These temperature contours provide insight into how the temperature evolves during different induction heating stages.

3.4 | Effect of Convective Heat Transfer Coefficient

As discussed in the problem definition, both radiative and convective heat transfer can play a pivotal role in the heat

rejection from the cylindrical object. Although the heat transfer coefficient arising from the radiation changes with time due to the rapid rise of surface temperature (Figure 5), the convective heat transfer coefficient (h_c) is not strongly related to surface temperature. However, one has better control over the convective heat transfer coefficient (h_c) because it can be modulated by modifying the fluid flow velocity around the object over an extensive range. To understand the thermal performance during induction heating, we studied convective heat transfer coefficient effects by varying it between zero and $1000 \text{ W/m}^2 \text{ K}$.

Figure 8 shows the temperature distribution for various h_c during induction heating at 500 s. Unlike the radiative heat transfer coefficient, which changes with time, the convective heat transfer coefficient remains constant for each individual case. As observed in Figure 8, there is a decrease in overall temperature within the cylinder as the convective heat transfer coefficient (h_c) is increased. In other words, the object achieves

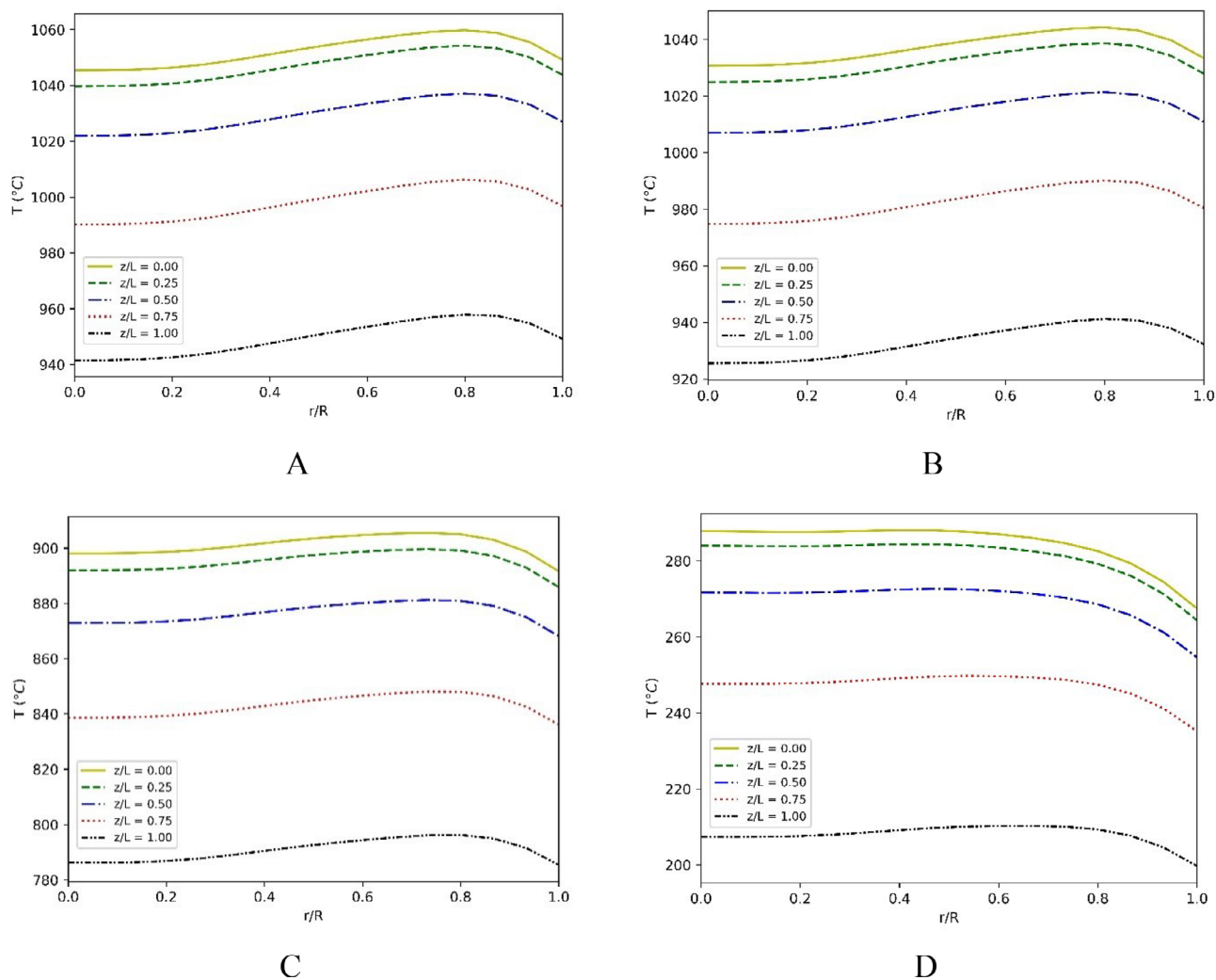


FIGURE 8 | The final temperature distribution inside a cylindrical object for 500 s of induction heating at 10 kHz frequency: (A) $h_c = 0 \text{ W/m}^2 \text{ K}$, (B) $h_c = 10 \text{ W/m}^2 \text{ K}$, (C) $h_c = 100 \text{ W/m}^2 \text{ K}$, and (D) $h_c = 1000 \text{ W/m}^2 \text{ K}$.

the highest temperature at the lower end of the convective heat transfer coefficient. For instance, when there is a zero or negligible level of convection heat transfer, object temperatures can exceed 1000°C locally. It is noteworthy to mention that the surface temperature remains nearly uniform in the radial direction (in Figure 8) because temperature profiles are presented much later in the induction heating process. The radial uniformity at the later stage of the induction heating is due to the high thermal conductivity of the conductive material and the shorter length scale in the radial direction for the problem considered here. However, radiative heat transfer is always present in induction heating, regardless of the value of the convective heat transfer coefficient. The magnitude of the radiative heat transfer coefficient eventually takes over as the dominating heat rejection mechanism during the later stage of heating, and it is responsible for the lower surface temperature compared to other regions in the r -direction. Although the final temperature distribution is nearly uniform in the radial direction, during the initial state of heating, a significant temperature gradient will be present in the radial direction, as shown in Figure 6A.

3.5 | Effect of AC Current Frequency and Amplitude

Induction heating uses electromagnetic energy through AC current flowing through an external electric coil. Two primary features of the AC currents are amplitude and frequency, which impact the volumetric heat generation term during heating. Thus, it is important to study AC current amplitude and frequency dependence on the overall heating process. Frequency selection is determined by different factors, such as specific applications, the size of the load, and the required penetration depth for heat treatment. Different frequencies are typically employed for forging, forming, melting, and surface hardening [49]. For example, at frequencies of about 1 and 3 kHz, the penetration depth is relatively deep, allowing for more uniform heating throughout the material, which is advantageous for processes requiring thorough heat distribution [50]. On the other hand, for frequencies around 7 kHz, the penetration depth is shallower, focusing the heating effect closer to the surface, which is ideal for applications requiring surface hardening [51]. In other words, frequency directly affects the penetration depth of the induced

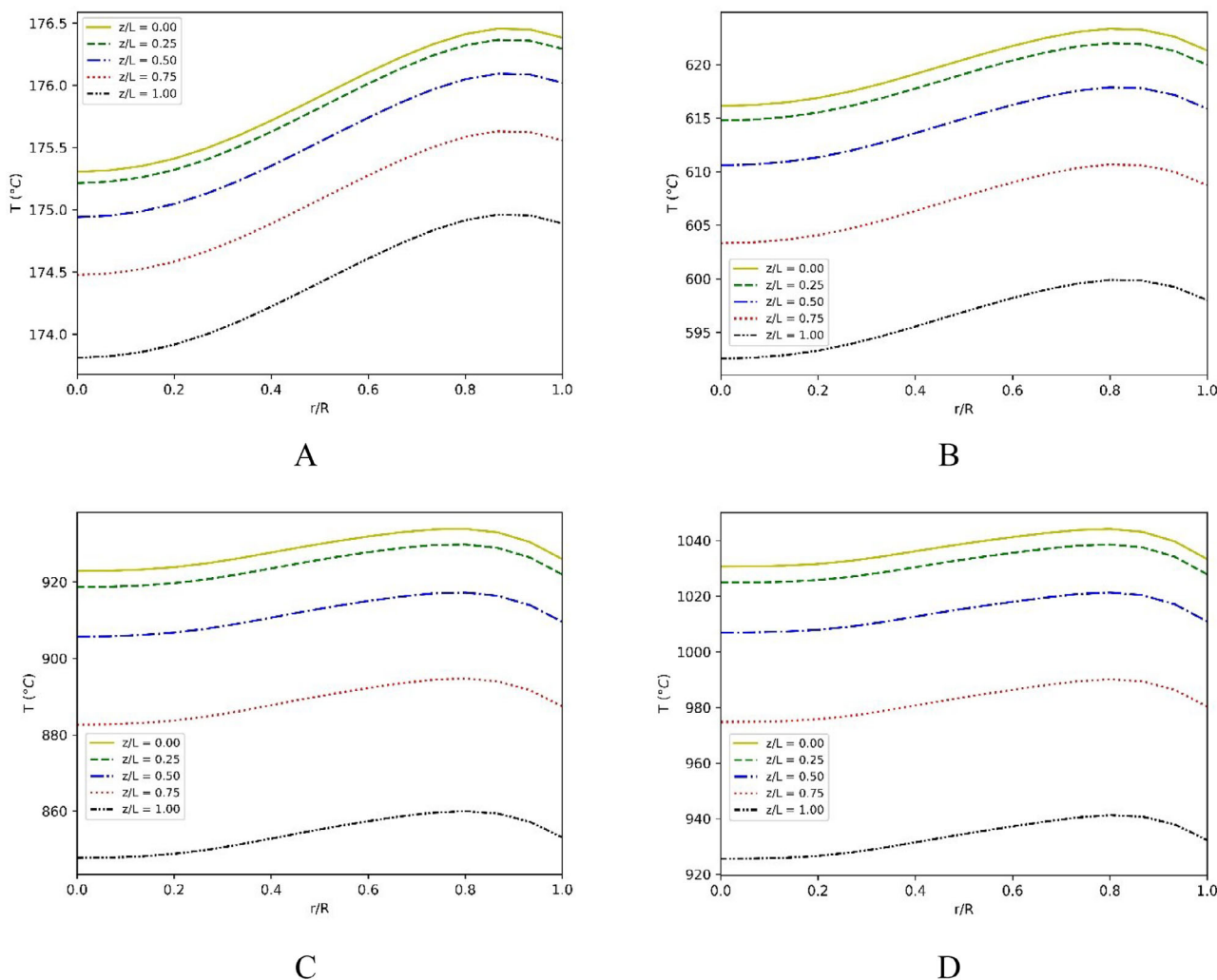


FIGURE 9 | The final temperature distribution for 500 s of induction heating of a cylindrical object at (A) $f = 1000$ Hz, (B) $f = 3000$ Hz, (C) $f = 7000$ Hz, and (D) $f = 10000$ Hz.

currents and the heating rate and, consequently, the overall temperature distribution within the object. One can better control the heating process by understanding how different frequencies impact these factors.

Figure 9 depicts the temperature distribution inside the cylinder for different frequency values ranging from 1000 to 10000 Hz. Our analytical results show higher temperatures at higher frequency cases due to the direct relationship between the volumetric heat generation term and the applied current frequency. As the applied frequency increases, the penetration depth of the electromagnetic wave decreases. At higher frequencies, the imposed magnetic field's direction changes so quickly that the induced currents in one direction hardly have enough time to penetrate into the depth of the material before their time is up. As a result, these currents are concentrated near the surface of the cylindrical object, causing a much higher volumetric heat generation close to the outer surface. Conversely, for lower frequency cases, the volumetric heat generation term is much smaller but spreads deeper in the radial direction. For 500 s of induction heating, both radial and axial temperature distribution is negligible at $f = 1$ kHz,

and lumped capacitance modeling can be used to simulate this kind of heating. However, the spatial temperature variation in the axial direction can reach close to 100°C for $f = 10$ kHz case. Thus, one must use multidimensional analysis for such a case of induction heating. Moreover, it is noteworthy to mention that, in all cases, the temperatures peak within 20% of the outer surface.

The effect of current density is also crucial in applications where precise temperature control is essential for ensuring quality and safety. The impact of changing the current density on the temperature variations inside the cylinder is illustrated in Figure 10 for two (RMS) current values, 276.38 and 467.72 A. These applied current values are based on the experimental study of identical induction heating work presented in [38]. As the current intensity increases, the heat generation increases, leading to higher overall temperatures within the cylinder. Furthermore, as expected, the temperature increases from the centerline to the surface of the cylinder, with higher temperatures at $z/L = 0$ and lower temperatures at $z/L = 1$. This trend is attributed to heat transfer from the sides as well as the top and bottom surfaces of the cylinder.

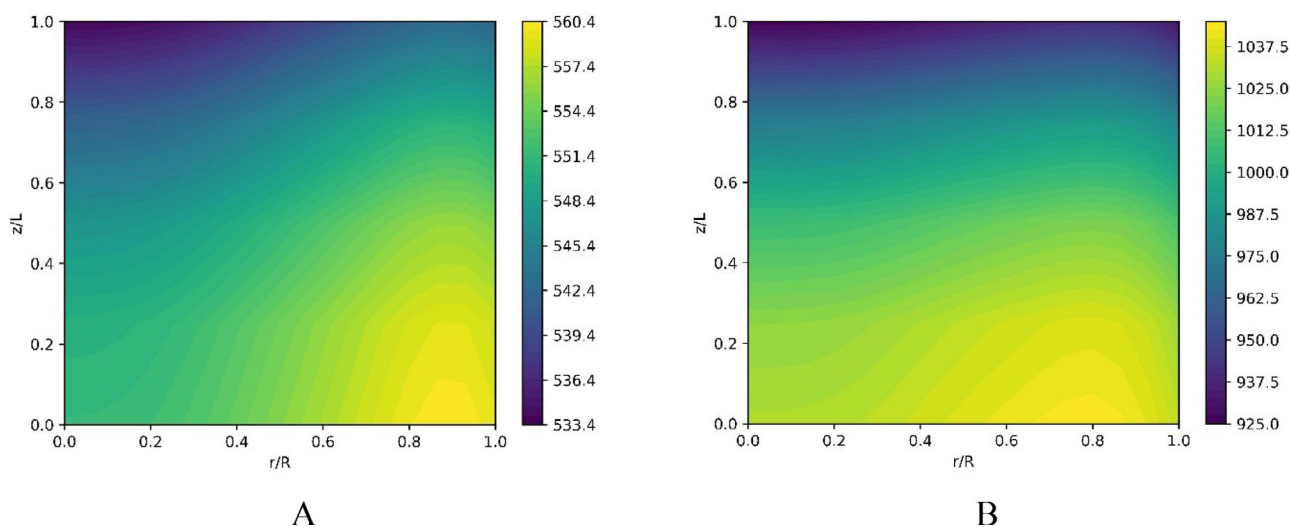


FIGURE 10 | The final temperature distribution for 500 s induction heating of a cylindrical object at (A) $I = 276.38$ A and (B) $I = 467.72$ A. Here, $f = 10$ kHz.

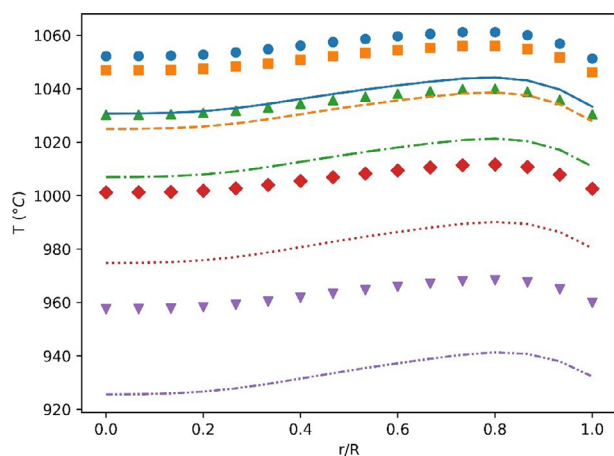


FIGURE 11 | The final temperature distribution for temperature-dependent and temperature-independent material properties (constant at 893.15 K) for 500 s of induction heating of a cylindrical object. Symbols represent temperature-independent properties, whereas lines denote temperature-dependent properties. The colors indicate: $z/L = 0.00$ (blue), $z/L = 0.25$ (orange), $z/L = 0.50$ (green), $z/L = 0.75$ (red), and $z/L = 1.00$ (purple).

The aforementioned observations highlight the significant roles of current intensity in determining thermal behavior during induction heating, providing valuable insights for optimizing heating parameters to achieve precise and efficient temperature control.

3.6 | Effect of Temperature-Dependent Properties

Finally, a comparative study is conducted to examine the impact of both temperature-dependent and independent material properties on temperature distribution during induction heating. Figure 11 presents the temperature results for both cases, where temperature-dependent results are shown by lines and temperature-independent values are presented by symbols. Con-

stant property values corresponding to 893.15 K were utilized for the temperature-independent properties. For all axial locations, a model based on the temperature-independent material properties predicted significantly higher temperature values than those of temperature-dependent material properties. This comparative analysis reveals how varying material properties (with temperature) affect the temperature distribution within the material. Due to significant differences in predicted temperature, one must use temperature-dependent properties in estimating temperature distribution.

4 | Conclusions

A closed-form analytical solution is provided for the distribution of temperature in a non-magnetic cylindrical object under induction heating by considering time-dependent boundary conditions and temperature-dependent material properties. In this analytical study, the Joule heat generated by the eddy current is obtained from the simplified Maxwell's equations, which is utilized as a source term in the 3D unsteady energy equation to determine the temperature distribution within the object. The non-homogenous heat equation is solved using Green's function method for temperature by employing separation of variables techniques. The resulting temperatures from the closed-form analytical solution are compared with data from an identical experimental study. Notably, our analytical solution shows a much better agreement with experimental observations than the lumped capacitance-based approach, highlighting its enhanced precision and effectiveness. The results of this study reveal that augmentation of the convective heat transfer coefficient reduces the overall temperature, with negligible convection leading to much higher temperatures. During the initial heating stage, there is a significant radial temperature gradient, which becomes more uniform over time because of the material's high thermal conductivity as well as the shorter length scale in the radial direction. At the later stage of induction heating, the magnitude of the radiative heat transfer coefficient becomes the primary mechanism for heat rejection, resulting in lower outer surface

temperatures compared to the core. These results highlight the critical role of convection control and the vital role of radiation in managing heat transfer during induction heating. In addition, this study shows that increasing frequency from 1 kHz to 10 kHz significantly raises the temperature inside the cylinder. Higher frequencies reduce the penetration depth of electromagnetic waves, causing a surface-level concentration of heat and resulting in higher surface temperatures. In contrast, lower frequencies lead to more uniform heat distribution due to higher penetration depth. For frequencies around 1 kHz, temperature variations are minimal, allowing simplified modeling, whereas at 10 kHz, significant spatial temperature differences require multidimensional analysis. It is also observed that increasing current intensity further enhances heat generation within the cylinder, leading to higher overall temperatures. Our analytical results also reveal that constant material properties significantly overpredict the temperature distributions within the object. This highlights the importance of considering temperature-dependent properties to accurately capture temperature distribution, as constant properties fail to capture the true thermal behavior.

Acknowledgments

This work was funded partly by the US National Science Foundation under grant number DGE 2244082.

Conflicts of Interest

The authors declare no conflicts of interest.

Data Availability Statement

The data supporting this study's findings are available from the corresponding author upon reasonable request.

References

- O. Lucia, P. Maussion, E. J. Dede, and J. M. Burdío, "Induction Heating Technology and Its Applications: Past Developments, Current Technology, and Future Challenges," *IEEE Transactions on Industrial Electronics* 61, no. 5 (2013): 2509–2520.
- E. Bellevrat and K. West, *Clean and Efficient Heat for Industry*, IEA Commentary, January 2018, Paris, IEA.
- J. Choi, S. Kim, K. Kim, M. Park, I. Yu, S. Kim, and K. Kim, "Design and Performance Evaluation of a Multipurpose HTS DC Induction Heating Machine for Industrial Applications," *IEEE Transactions on Applied Superconductivity* 25, no. 3 (2015): 3700105.
- R. Joshi, R. S. Perala, M. Srivastava, B. P. Singh, and R. S. Ningthoujam, "Heat Generation From Magnetic Fluids Under Alternating Current Magnetic Field or Induction Coil for Hyperthermia-Based Cancer Therapy: Basic Principle," *Journal of Radiation and Cancer Research* 10, no. 4 (2019): 156–164.
- A. Mühlbauer, *History of Induction Heating and Melting* (Germany: Vulkan-Verlag GmbH, 2008).
- R. Musii, P. Pukach, I. Kohut, M. Vovk, and L. Šlahor, "Determination and Analysis of Joule's Heat and Temperature in an Electrically Conductive Plate Element Subject to Short-Term Induction Heating by a Non-Stationary Electromagnetic Field," *Energies* 15, no. 14 (2022): 5250.
- V. Rudnev, D. Loveless, and R. L. Cook, *Handbook of Induction Heating* (Boca Raton, FL: CRC Press, 2017).
- H. Kurose, D. Miyagi, N. Takahashi, N. Uchida, and K. Kawanaka, "3-D Eddy Current Analysis of Induction Heating Apparatus Considering Heat

- Emission, Heat Conduction, and Temperature Dependence of Magnetic Characteristics," *IEEE Transactions on Magnetics* 45, no. 3 (2009): 1847–1850.
- C. J. Erickson, C. D. Potts, and B. M. Jones, "Electrical and Electronics Engineering," *Power Electron* 15 (1999): 85.
- N. Tsopelas and N. J. Siakavellas, "Influence of Some Parameters on the Effectiveness of Induction Heating," *IEEE Transactions on Magnetics* 44, no. 12 (2008): 4711–4720.
- A. Morandi and M. Fabbri, "In-Depth Induction Heating of Large Steel Slabs by Means of a DC Saturating Field Produced by Superconducting Coils," *IEEE Transactions on Applied Superconductivity* 26, no. 4 (2016): 1–7.
- H. M. El-Mashad and Z. Pan, "Application of Induction Heating in Food Processing and Cooking," *Food Engineering Reviews* 9 (2017): 82–90.
- G. Francesco, A. Giuseppina, and F. Luigino, "Incremental Forming With Local Induction Heating on Materials With Magnetic and Non-Magnetic Properties," *Procedia Engineering* 183 (2017): 143–148.
- F. N. Shang, E. Sekiya, and Y. Nakayama, "Application of High-Frequency Induction Heating Apparatus to Heat Treatment of 6061 Aluminum Alloy," *Materials Transactions* 52, no. 11 (2011): 2052–2060.
- A. Khersonsky and H. Lee, "Induction Heating for Efficient Laser Applications," *Advanced Materials and Processes* 157, no. 4 (2000): 39.
- M. Róžański and P. Rekasowski, "Application of Induction Heating in Brazing Processes," *Welding International* 26, no. 4 (2012): 282–285.
- S. Aslan, M. Ozturk, and N. Altintas, "A Comparative Evaluation of Wide-Bandgap Semiconductors for High-Performance Domestic Induction Heating," *Energies* 16, no. 10 (2023): 3987.
- P. Vishnuram, G. Ramachandiran, S. Ramasamy, and S. Dayalan, "A Comprehensive Overview of Power Converter Topologies for Induction Heating Applications," *International Transactions on Electrical Energy Systems* 30, no. 10 (2020): e12554.
- M. N. Pérez-Camacho, J. Abu-Dahrieh, D. Rooney, and K. Sun, "Biogas Reforming Using Renewable Wind Energy and Induction Heating," *Catalysis Today* 242 (2015): 129–138.
- Y. T. Kim, J. J. Lee, and J. Lee, "Electricity-Driven Reactors That Promote Thermochemical Catalytic Reactions via Joule and Induction Heating: A Review," *Chemical Engineering Journal* 470 (2023): 144333.
- V. Suru, M. Popescu, and A. Bitoleanu. Energetic Performances of Induction Heating Systems With Voltage Resonant Inverter. in 2013 4th International Symposium on Electrical and Electronics Engineering (ISEEE) (Piscataway, NJ: IEEE, 2013), 1–6.
- X. Wu, C. Li, S. Sun, R. Tong, and Q. Li, "A Study on the Heating Method and Implementation of a Shrink-Fit Tool Holder," *Energies* 12, no. 18 (2019): 3416.
- H. Hammi, A. El Ouafi, N. Barka, and A. Chebak, "Scanning Based Induction Heating for AISI 4340 Steel Spline Shafts-3D Simulation and Experimental Validation," *Advances in Materials Physics and Chemistry* 7, no. 6 (2017): 263–276.
- H. R. Ban, K. T. Yu, J. H. Lee, et al., "Analytical and Experimental Study of Electromagnetic Loss and Temperature Rise in Induction Machines," *Advances* 14, no. 3 (2024): 035101.
- M. Niu, T. Akiyama, R. Takahashi, and J. I. Yagi, "Experimental and Parametric Analyses of Heat Transfer Within Two-Layered Packed Beds of Iron and Graphite in a High-Frequency Induction Furnace," *Tetsu-to-Hagané* 82, no. 2 (1996): 105–110.
- P. E. Aba-Perea and E. Becker, "Measurement and Modeling of Thermal Evolution During Induction Heating and Thixoforming of Low Carbon Steel," *Journal of Materials Processing Technology* 283 (2020): 116717.
- E. Tharmapalan, S. Sivalingam, N. M. Seyyaf, N. Kanagalingam, L. C. Balasooriya, and I. D. Nissanka, "Performance Improvement of Indus-

- trial Induction Mould Heating Oven,” in 2020 Moratuwa Engineering Research Conference (MERCon) (Moratuwa, Srilanka: IEEE, 28–30 July 2020), 602–607.
28. M. C. Song and Y. H. Moon, “Coupled Electromagnetic and Thermal Analysis of Induction Heating for the Forging of Marine Crankshafts,” *Applied Thermal Engineering* 98 (2016): 98–109.
29. S. Yin and X. Ma, “Analytical Model for the Equivalent Impedances of the Domestic Induction Heating System With Rectangular Cross-Sectional Windings,” *IET Science, Measurement & Technology* 13, no. 7 (2019): 1026–1032.
30. P. Herasymenko, “Study of the Suitable Value of Dead-Time Between Control Signals of Transistors for a Series-Resonant Inverter With Phase-Shift Control in Induction Heating Systems,” *EUREKA: Physics and Engineering* 3 (2021): 60–70.
31. J. Wang, Q. Liu, Y. J. Liu, B. Shi, Y. D. Bao, and L. J. Zhang, “The Design and Simulation of Circuit for Electromagnetic Force Assisted Line Heating Device,” *Advances in Materials Research* 652 (2013): 2010–2018.
32. M. Areitioaurtena, U. Segurajauregi, V. Akujärvi, M. Fisk, I. Urresti, and E. Ukar, “A Semi-Analytical Coupled Simulation Approach for Induction Heating,” *Advanced Modeling and Simulation in Engineering Sciences* 8, no. 1 (2021): 14.
33. J. H. Lee, K. H. Lee, and J. S. Yun, “An Electromagnetic and Thermo-Mechanical Analysis of High Frequency Induction Heating for Steel Plate Bending,” *Key Engineering Materials* 326 (2006): 1283–1286.
34. M. Ostroushko, A. Buchau, and W. Rucker, “Design and Simulation of the Electromagnetic Heating of a Biological Tissue,” *COMPEL - The International Journal for Computation and Mathematics in Electrical and Electronic Engineering* 36, no. 2 (2017): 408–416.
35. B. Patidar, M. M. Hussain, S. K. Jha, A. Sharma, and A. P. Tiwari, “Analytical, Numerical and Experimental Analysis of Induction Heating of Graphite Crucible for Melting of Non-Magnetic Materials,” *IET Electric Power Applications* 11, no. 3 (2017): 342–351.
36. F. Li, J. Ning, T. Wang, and S. Y. Liang, “Analytical Modeling and Sensitivity Analysis of the Temperature Distribution in the Planar Scanning Induction Heating Based on 2D Moving Heat Source,” *Journal of Mechanical Science and Technology* 33 (2019): 5093–5102.
37. F. Li, J. Ning, and S. Y. Liang, “Analytical Modeling of the Temperature Using Uniform Moving Heat Source in Planar Induction Heating Process,” *Applied Sciences* 9, no. 7 (2019): 1445.
38. T. A. Jankowski, N. H. Pawley, L. M. Gonzales, C. A. Ross, and J. D. Journey, “Approximate Analytical Solution for Induction Heating of Solid Cylinders,” *Applied Mathematical Modelling* 40, no. 4 (2016): 2770–2782.
39. A. Abdi, Y. Ouazir, G. Barakat, and Y. Amara, “Permanent Magnet Linear Induction Heating Device: New Topology Enhancing Performances,” *COMPEL - The International Journal for Computation and Mathematics in Electrical and Electronic Engineering* 37, no. 5 (2018): 1755–1767.
40. R. Musii, P. Pukach, N. Melnyk, M. Vovk, and L. U. Šlahor, “Modeling of the Temperature Regimes in a Layered Bimetallic Plate Under Short-Term Induction Heating,” *Energies* 16, no. 13 (2023): 4980.
41. J. Davies, “Conduction and Induction Heating,” IET; (London, UK: Published by Peter Peregrinus Ltd, 1990), 978-0-86341-174-8.
42. M. W. Kennedy, S. Akhtar, J. A. Bakken, and R. E. Aune, “Empirical Verification of a Short-Coil Correction Factor,” *IEEE Transactions on Industrial Electronics* 61, no. 5 (2013): 2573–2583.
43. R. W. Hornbeck, *Numerical Marching Techniques for Fluid Flows With Heat Transfer* (Washington, DC: Scientific and Technical Information Office, National Aeronautics and Space Administration, 1973).
44. *Properties and Characteristics of Graphite* (Decatur, TX: POCO Graphite Inc., 1994).
45. M. R. Hossan, D. Byun, and P. Dutta, “Analysis of Microwave Heating for Cylindrical Shaped Objects,” *International Journal of Heat & Mass Transfer* 53, no. 23–24 (2010): 5129–5138.
46. M. R. Hossan and P. Dutta, “Effects of Temperature Dependent Properties in Electromagnetic Heating,” *International Journal of Heat & Mass Transfer* 55, no. 13–14 (2012): 3412–3422.
47. K. B. Mani, M. R. Hossan, and P. Dutta, “Thermal Analysis of Microwave Assisted Bonding of Poly (Methyl Methacrylate) Substrates in Microfluidic Devices,” *International Journal of Heat & Mass Transfer* 58, no. 1–2 (2013): 229–239.
48. X. Zhou and B. G. Thomas, “Measuring Heat Transfer During Spray Cooling Using Controlled Induction-Heating Experiments and Computational Models,” *Applied Mathematical Modelling* 37, no. 5 (2013): 3181–3192.
49. E. J. Davies and P. G. Simpson, “Induction Heating for Industry,” *Electron Power* 25, no. 7 (1979): 508–515.
50. V. Rudnev, G. A. Fett, A. Griebel, and J. Tartaglia, “Principles of Induction Hardening and Inspection,” in *Induction Heating and Heat Treatment ASM International* (Almere, The Netherlands: ASM International, 2014), 58–86.
51. C. Mich-Vancea, T. Leuca, and S. Nagy, “A Study Regarding the Efficiency of the Electromagnetic Induction Thermal Treatment Process Depending to the Work Frequency,” *Journal of Electrical and Electronic Engineering* 4, no. 1 (2011): 109–112.